Radiobrightness of Diurnally Heated, Freezing Soil

A. W. England

Radiation Laboratory

Department of Electrical Engineering

and Computer Science

The University of Michigan

Ann Arbor, MI 48109-2122

August 15, 1989

Abstract

Freezing and thawing soils exhibit unique radiometric characteristics. To examine these characteristics, diurnal insolation is modeled as 1-dimensional heating of a moist soil halfspace during a typical fall at a northern Great Plains site (Bismarck, ND). The 1-dimensional, heat flow equation is non-linear because both the enthalpy and the thermal conductivity of freezing soils are non-linear functions of temperature. The problem is particularly difficult because phase boundaries propagate in time, and because soils that contain clay freeze over a range of temperatures rather than at 0° C--that is, they possess diffuse phase boundaries.

A modified Chernous'ko method was used to integrate the heat flow equation to obtain monthly thermal models during a typical September through December period. Diurnal radiobrightness curves at 10.7, 18, and 37 GHz were computed for each month. The 37 GHz radiobrightness best tracks soil surface temperature, the 10.7-37 GHz spectral gradient of thawed soils is strongly positive, the spectral gradient of frozen soils is slightly negative, and the midnight to noon spectral gradient is shifted by approximately +0.1 K/GHz by diurnal changes in the surface temperature and the thermal gradient. These observations support the use of SMMR's 37 GHz radiobrightness and its 10.7-37 GHz spectral gradient as discriminants in a frozen soil classifier for high latitude prairie.

Introduction

The quantity and state of moisture in soil can be estimated from satellite radiobrightness signatures. There is a large body of literature linking moisture content to radiobrightness [1]-[6]. Whether or not the soil is frozen affects the rate of energy transfer to the atmosphere by limiting evapotranspiration, and affects the rainfall or snowmelt runoff potential by reducing the infiltration capacity of the soil. Zuerndorfer et al. [7] produced freeze/thaw maps of the northern Great Plains

from Nimbus 7 Scanning Multichannel Microwave Radiometer (SMMR) data. This paper is an examination of the theoretical basis for microwave radiometric, frozen soil classification.

Figures 1a and 1b illustrate the observational basis for a frozen soil classifier. A 37 GHz radiobrightness below about 247 K indicates frozen soil, and one above about 247 K indicates thawed soil for Bismarck, ND. However, regions near the Missouri River, Sakakawea and Devils Lakes, the Red River Valley, and in the wakes of a regional rainfall often appear anomalously cold at 37 GHz because of exceptional wetness for the northern Great Plains. The confusing factor is that 37 GHz radiobrightness, while least sensitive to moisture of the SMMR frequencies, is darkened by moisture. A second discriminant -- the 10.7-37 GHz spectral gradient -- resolves the ambiguity because frozen soils are observed to have negative spectral gradients, and moist soils are generally observed to have a positive spectral gradient. Figures 1a and 1b also exhibit an upward shift in the spectral gradient between midnight and noon of about 0.1 K/GHz.

A valid theoretical model should replicate the behavior of the 37 GHz radiobrightness, the dominant characteristics of the 10.7-18-37 GHz spectral gradient, and the diurnal shifts in the spectral gradient during the September through December months in the northern Great Plains. Model parameters will be chosen for prairie near Bismarck, ND.

1-Dimensional Heat Flow

The 1-dimensional heat flow equation for temperature T (Kelvin), depth z (cm), and time t (sec) is [8]

$$\frac{\partial E(T)}{\partial t} = - \frac{\partial F(z,t)}{\partial z} \qquad (1)$$

where E(T) is enthalpy (cal/cm^3) and F(z,t) is heat flux (cal/cm^2-K) (T is a function of z and t). Heat flux is linearly related to the temperature gradient, $\partial T/\partial z$, by

$$F(z,t) = - K(T) \frac{\partial T}{\partial z} \tag{2}$$

where K(T) is thermal conductivity (cal/cm-sec-K). That is,

$$\frac{\partial E(T)}{\partial t} = \frac{\partial}{\partial z}\left(K(T)\frac{\partial T}{\partial z}\right) \tag{3}$$

With respect to a reference temperature, T_o, E(T) is generally the linear function

$$E(T) = \rho\, c_p \left(T - T_o\right) \tag{4}$$

where ρ is density (gm/cm^3), and c_p is specific heat at constant pressure (cal/gm-K). If K(T) is constant, Equation (3) becomes the parabolic linear differential equation

$$\frac{\partial T}{\partial t} = \kappa \frac{\partial^2 T}{\partial z^2} \tag{5}$$

where constant κ is thermal diffusivity (cm^2/sec)

$$\kappa = \frac{K}{\rho\, c_p} \tag{6}$$

Equation (5) can be solved analytically by either the harmonic or the Laplace methods [8], or by a finite difference numerical method. Watson used the Laplace method [9][10], and Kahle used the finite difference method [11] to develop thermal models for the diurnal insolation of rock and soil. Their models relate day-night differences in thermal infrared temperature to rock and soil type. However, if soils freeze or thaw diurnally, then Equation (3) is not linear and is not amenable to either the Watson or the Kahle methods.

Equation (3) looks simpler with the substitution of variables

$$u = \int_{T_0}^{T} K'(\tau)\, d\tau \tag{7}$$

so that u = u(T) and Equation (3) becomes

$$\frac{\partial E(T)}{\partial t} = \frac{\partial^2 u}{\partial z^2} \tag{8}$$

This 1-dimensional, non-linear, heat flow equation is called Stefan's problem [12], and there are three ways to solve it: The finite difference method [13], the moving boundary method [14], and the isotherm propagation or Chernous'ko method [15]. The finite difference method for non-linear problems suffers from uncertain convergence properties. The moving boundary method involves seeking analytical solutions to the linear regions on either side of moving phase boundaries. This method is particularly awkward if the phase change occurs over a depth zone, as in freezing soils, rather than at a plane interface, or if there are multiple freezing isotherms, as in the periodic heating case. The Chernous'ko method has a problem with the periodic heating case.

Chernous'ko [15] replaced E(T) with the piecewise constant approximation, H(T), (shown schematically in Figure 2a)

$$H(T) = E(T_n) \quad \text{for} \quad T_n \le T < T_{n+1} \tag{9}$$

where T_n denotes isotherm n ordered by increasing depth. While these isotherms can be any temperature, integer values of Kelvin are convenient. The slope of the linear portions of E(T) below 268 K and above 273 K are the ρc_p for frozen and moist soils, respectively. The increased slope between 268 and 273 K results from the latent heat of melting of moisture in the soil (linearity of E(T) in this region is an approximation). In this example, melting occurs over 5 degrees. For sandy soils, the range might be near 1 degree; for some clay soils, it might be more than 10 degrees [16].

In terms of H(T), Equation (9) becomes

$$\frac{\partial H(T)}{\partial t} = \frac{\partial^2 u}{\partial z^2} \tag{10}$$

Locally constant H requires that u be a linear function of z between isotherms T_n and T_{n+1}, i.e.,

$$u = u_n + \frac{u_{n+1}-u_n}{z_{n+1}-z_n}(z - z_n) \tag{11}$$

where z_n is the depth of isotherm T_n.

If the value of H(T) at $z > z_n$ is denoted by H^+, and H(T) at $z < z_n$ is H^-, then Equation (10) can be integrated at constant time along path a-b in Figure 3,

$$\frac{\partial}{\partial t}\int_a^b H(T)\,dz = \left(\frac{\partial u}{\partial z}\right)_{b,t} - \left(\frac{\partial u}{\partial z}\right)_{a,t} \tag{12}$$

to yield

$$\frac{\partial}{\partial t}\left[H^+(b-z_n) + H^-(z_n-a)\right] = \left(\frac{\partial u}{\partial z}\right)_{b,t} - \left(\frac{\partial u}{\partial z}\right)_{a,t} \tag{13}$$

From Equation (11), because z_n is the only function of time on the left of Equation (13),

$$\frac{dz_n}{dt} = \frac{1}{(H^- - H^+)}\left\{\left(\frac{u_{n+1}-u_n}{z_{n+1}-z_n}\right) - \left(\frac{u_n-u_{n-1}}{z_n-z_{n-1}}\right)\right\} \tag{14}$$

Equation (14) is the ordinary, linear differential equation that Chernous'ko used to propagate each isotherm in time.

Equation (14) fails in the periodic heating problem because of an asymmetry in H(T) between heating and cooling. For example, consider the propagation of isotherm z_n where $T_{n-1} < T_n = T_{n+1}$. In this case, $H^+ > H^-$ and

$$\frac{dz_n}{dt} = \frac{-1}{(H^- - H^+)} \left\{ \left(\frac{u_n - u_{n-1}}{z_n - z_{n-1}} \right) \right\} \tag{15}$$

However, if $T_{n-1} > T_n = T_{n+1}$, then $H^+ = H^-$ and dz_n/dz in Equation (14) is undefined. This asymmetry can be ameliorated by substituting the piecewise constant H(T) shown schematically in Figure 2b, i.e.,

$$H(T) = \left\{ \begin{array}{ll} \frac{E(T_n)+E(T_{n+1})}{2} & \text{for } T_n < T < T_{n+1} \\ E(T_n) & \text{for } T = T_n \\ \frac{E(T_{n-1})+E(T_n)}{2} & \text{for } T_{n-1} < T < T_n \end{array} \right\} \tag{16}$$

Isotherm propagation with this alternative approximation for E(T) will be referred to as the modified Chernous'ko method.

Boundary Conditions

Watson [9] and Kahle [11] used boundary conditions for the energy flux, $F_{net}(z)$,

$$F_{net}(0) = F_{sun} + F_{sky} + F_{wind} - F_{ground}$$

$$F_{net}(\infty) = 0 \tag{17}$$

where z = infinity means depths greater than the penetration of the diurnal thermal pulse. The parameters that comprise these boundary conditions for Bismarck, ND, are described in Table 1. F_{sun} is insolation reduced by cloud cover, atmospheric absorption, albedo, and the cosine of the

zenith angle. F_{sky} is sky brightness plus a small correction for cloud cover. F_{wind} is a small correction for sensible heat transfer between ground and air used by Kahle [11]. F_{ground} is gray-body emission from the soil's surface. Topography and evapotranspiration are ignored.

Radiobrightness

Consider thermal microwave emission from volume, dV, within a dielectric halfspace (Fig 4). The energy, dQ, arriving at surface element, dA, is

$$dQ = E\,dV\; e^{-2\beta z/\cos\theta'} \frac{dA}{z/\cos\theta'} \tag{18}$$

where 2β is the power loss coefficient,

$$2\beta = \frac{2\pi\sqrt{\varepsilon'}\tan\delta}{\lambda_o} \tag{19}$$

ε' is the real part of the dielectric constant, $\tan\delta$ is the loss tangent, λ_o is free-space wavelength, and E is volume emissive power for dV at thermal temperature, T(z),

$$E = \varepsilon'\, 2\beta\, T(z). \tag{20}$$

With $dV = z\,d\omega\,dz/\cos\theta'$, and with a first order approximation for T(z), the intensity, dI', below the interface in direction θ' is

$$dI' = \varepsilon'\, 2\beta\, \{T_g + (\frac{\partial T}{\partial z})_o z\}\;\; e^{-2\beta\, z/\cos\theta'} dz/\cos\theta' \tag{21}$$

where T_g is soil surface temperature, and I' has been normalized by Planck's coefficient so that its dimension is Kelvin. Integration of Equation (21) yields the upwelling intensity below the interface

$$I' = \varepsilon' \{T_g + \frac{\cos\theta'}{2\beta} (\frac{\partial T}{\partial z})_o\} \tag{22}$$

If reflected sky-brightness and atmospheric absorption and emission are ignored, the normalized intensity above the interface (the radiobrightness, T_b) is $e(\lambda, \theta)\ I'(\theta')/\varepsilon'$, where $e(\lambda, \theta)$ is the directional spectral emissivity and the source of the emission polarization. Because of Snell's Law effects, cos θ' below the interface is relatively near to unity for most satellite incidence angles, θ (typically < 50°). With only a slight loss of generality, we shall assume that θ=0 so that polarization can be ignored, and so that brightness temperature can be written

$$T_b = e(\lambda)\ \{T_g + z_e \left(\frac{\partial T}{\partial z}\right)_o\} \tag{23}$$

where $z_e = (2\beta)^{-1}$ has the dimension of length. z_e should be called the effective emitting depth. It is equivalent to one optical depth in optics, or to half the skin depth in electromagnetics.

The dielectric properties of typical freezing soils at microwave frequencies are given by Hoekstra and Delaney [16]. Figure 5, from their paper, shows the variability in the complex dielectric constant for several moisture percentages in Groodrich clay and in Fairbanks silt. Note that the dielectric properties are essentially constant through freezing for a moisture content of 5%. This insensitivity to temperature for small moisture contents occurs because the water is chemisorbed, or adsorbed, to the clay or sand interfaces within the soil [17] and are not free to rotate with the electromagnetic wave. A reasonable approximation to the complex dielectric properties of moist soil, ε^*, through freezing is

$$\varepsilon^* = \varepsilon^*_{soil} + \frac{(m-0.07)}{(1-m)}\,\rho\ \{f\,\varepsilon^*_{water} + (1-f)\,\varepsilon^*_{ice}\} \tag{24}$$

where ε^*_{soil} = dielectric constant of 7% moist soil

$$\varepsilon^*_{water} = n^2 + \frac{K_s - K_\infty}{1+(j\omega\tau_1)^{1-\alpha}} + \frac{K_\infty - n^2}{1+j\omega\tau_2} \qquad [18][19]$$

$$n^2 = 1.8$$

$$K_S = 295.68 - 1.2283\,T + 2.094\times10^{-3}\,T^2 - 1.41\times10^{-6}\,T^3$$

$K_\infty = 4.2$

$\alpha = 0.012$

$\tau_1 = 5.62 \times 10^{-15}\, e^{0.188/kT}$ sec

$\tau_2 = 4.2 \times 10^{-14}$ sec

T = temperature Kelvin

k = Boltzmann's constant = 8.61735×10^{-5} eV/K

ω = angular frequency, radians/sec

$$\varepsilon^*_{ice} = K_\infty + \frac{K_S - K_\infty}{1 + j\omega\tau}$$

$K_\infty = 3.2$

$K_S = 3.2 + 20715/(T-38)$ [20]

$\tau = 4.76 \times 10^{-16}\, e^{0.577/kT}$ [21].

The Model

Appropriate model parameters for prairie near Bismarck are listed in Table 2. Parametric variables in these models are date and moisture content. While it might be argued that all parameters should be examined parametrically, the extensive computation required is not warranted by any possibility of inverting radiobrightness data to obtain more than moisture content or state.

The initial temperature of the thermal model was estimated from the average, diurnal radiation balance,

$$\theta\, \sigma\, T_{og}^4 = \frac{1}{24} \int_{24\ hr} (F_{sun} + F_{sky})\, dt \qquad (25)$$

where T_{og} becomes the initial temperature. T_{og} isotherms were placed at each centimeter of depth, and then propagated subject to the boundary conditions. The propagation time interval was assignable, but typically 6 seconds, and each 24 hour iteration began at midnight. The solution

was declared to have converged when the maximum surface temperature difference for each minute between 24 hour iterations was less than 0.001 Kelvins. Convergence required between eight and twelve iterations depending upon the month, the soil moisture content, and the propagation interval.

Observations

Temperature versus depth profiles at midnight, 6:00 a.m., noon, and 6:00 p.m. for Bismarck, ND, are shown in Figure 7. The gross features of these profiles are relatively independent of moisture content and month. Among these four profiles, surface temperatures are coldest at 6:00 a.m. (predawn) and hottest at noon as expected, and thermal pulses at depth are most pronounced at 6:00 p.m. Thermal gradients at the surface are always positive at midnight, 6:00 a.m., and 6:00 p.m., and they are always negative at noon. Note that the effect of freezing and thawing during October through December is a general compression of the temperature profile. That is, the apparent thermal inertia would be greater during freezing and thawing.

Figure 8 shows diurnal surface temperatures for September through December. The September curves, because temperatures are above freezing, look like the curves for diurnally heated, moist soils [9][10][11]. While moisture tends to reduce the day-night temperature difference, the effect is small. The October curves are very different. The daytime peak is lower because of reduced insolation, but nighttime curves are "held up" by the latent heat of fusion of soil moisture. The effects are similarly pronounced in November and December except that daytime peaks appear suppressed. The cause is the same -- daytime radiant heat goes into melting soil ice rather than into raising soil temperature. Again, an observable effect would be a strong increase in the apparent thermal inertia of freezing and thawing soils.

Effective emitting depths, z_e, as functions of microwave frequency, moisture content, and time-of-day are shown in Figure 9. The variability with frequency is caused by the Debye

relaxation processes in water and ice [16][17]. The September curves show the effects of moisture: The emitting depth of moist soil decreases with frequency, decreases with moisture content, and increases with insolation (maximum soil surface temperature) for frequencies below the primary relaxation frequency of water. The curves for October are dramatically different because ice in soil is effectively transparent to microwaves. Note that, for these model parameters, October near Bismarck is cold enough to completely freeze 10% and 15% moist soils, but not sufficiently cold to completely freeze 20% moist soil. The relatively smooth transitions between frozen and thawed emitting depths result from the assigned 3 degree freezing range of soil in this model. A reduced freezing range would cause a more abrupt transition.

The curves for November and December are mutually similar. Their major features are that the widths of the daytime melt period diminish slightly with increased moisture content because more of the daytime insolation must go into melting ice before temperatures rise. The slight increases in emitting depths with water content for the frozen periods occur because ice is more transparent to microwaves than the rock it replaces. The significant features of these curves are that microwave thermal emission originates much deeper in frozen soils than in moist soils, and that, for the SMMR frequencies, frozen soil emitting depths are roughly 1 cm and less. Therefore, frozen soil thermal gradients that are significant over depths of 1 cm should influence the SMMR spectral gradient.

Radiobrightness curves at the 10.7, 18, and 37 GHz SMMR frequencies, as functions of moisture content and time-of-day, are shown in Figure 10. The September (moist soil) brightness decreases with moisture content, and increases with microwave frequency. The frozen soil brightness curves during October through December are generally high and are relatively independent of microwave frequency. Midnight-noon differences are always positive for moist soils, and generally negative for diurnally thawing soils. While none of these soil models remain completely frozen throughout the day, a choice of parameters that avoids midday thawing would exhibit a positive midnight-noon shift in the spectral gradient. Of the three frequencies, the 37

GHz radiobrightness is least affected by moisture content or by freezing and thawing. That is, the 37 GHz radiobrightness most closely follows thermal temperature. It is this property that justifies its use as one of two discriminants in a SMMR, frozen soil classifier [7].

Radiobrightness spectral gradients, as functions of moisture content and time-of-day, are shown in Figure 11. The moist soil model gradients are always strongly positive, and the frozen soil model gradients are weakly negative. This unambiguous correlation is the reason that spectral gradient was chosen as a second discriminant in the SMMR, frozen soil classifier. SMMR observations are not universally unambiguous -- summertime, hot day SMMR data often exhibit negative gradients. However, summertime exceptions are unlikely to confuse a frozen soil classification.

The midnight and noon surface thermal gradients in Figure 7 are typically +1.5 and -3.5 degree/cm, respectively. This -5 degree/cm midnight-noon shift in the thermal gradient contributes about +0.1 K/GHz to the model's +0.5 to +1.4 K/GHz shift in the spectral gradient for the frozen soils shown in Figure 11. The preponderance of the shift is caused by the basic moist soil/frozen soil differences in spectral gradient. Note that the midnight-noon shift for moist soils (September) is negative.

Discrepancies

Model results are highly consistent with the SMMR observations reported by Zuerndorfer et al. [7]. However, there are three discrepancies: The SMMR frozen soil spectral gradient tends to be around -0.3 K/GHz, while the model predicts something like -0.1 K/GHz; the SMMR midnight-noon differences in spectral gradient for thawed soils average +0.2 K/GHz, while the model predicts that thawed soil differences should be weakly negative; and the SMMR moist soil spectral gradient can be negative on hot, summertime days, while the model predicts positive gradients.

While these discrepancies are ancillary to our objective of examining the performance of the 37 GHz radiobrightness and the 10.7-18-37 GHz spectral gradient as discriminants in a frozen soil classifier, they do suggest that the model is incomplete in that it ignores volume scatter darkening by prairie grasses and crop stubble, and by inhomogeneities within the frozen soil. The scattering albedo, ω_0, is a measure of the strength of volume scatter darkening. The parameter was used by Chandrasekhar [22] to describe darkening in planetary atmospheres, and applied by England [23][24] to describe darkening in frozen soils, ice, snow, and dry, planetary regoliths. It has become a parameter in most theories of wave propagation and scattering, e.g., Ishimaru [25]. For single scattering [25],

$$\omega_0 = \frac{N\sigma}{N\sigma + 2\beta} \tag{26}$$

where N is the number of scatterers per unit volume, σ is the scattering cross section for a single scatterer, and 2β is the power loss coefficient defined in Equation (19). For spherical scatterers whose diameters are small fractions of a wavelength (Raleigh scatterers),

$$\sigma \alpha \lambda^{-4} \tag{28}$$

so that ω_0 increases with decreasing wavelength to yield a negative spectral gradient of radiobrightness -- a "law of darkening". This short wavelength darkening is the likely cause of the strongly negative spectral gradient observed in SMMR data for frozen terrain.

The hot-day, negative spectral gradient may occur when heat drives most water from the canopy and from the upper layers of soil. Dry soils have an increased effective emitting depth so that volume scatter darkening may again cause a negative spectral gradient.

The discrepancy between observed and modeled, midnight-noon shifts in moist soil, spectral gradients may be caused by moisture (dew) on the plant canopy at midnight. However, without experimental studies, such explanations are only speculation.

Conclusions

A modified Chernous'ko method for solving Stefan's problem yields an acceptably rapid convergence to a solution for the thermal structure of diurnally insolated, moist and frozen soil. The modification involves an alternative, piecewise constant enthalpy-temperature approximation. With that modification, solutions exhibit the expected symmetry for heating and cooling.

Among the 10.7, 18, and 37 GHz SMMR frequencies, both the SMMR observations and the model show that the 37 GHz radiobrightness best tracks the thermal temperature of the soil's surface, and show that the 10.7-18-37 GHz spectral gradient is always negative for frozen soils. Therefore, the "and" condition, that the 37 GHz radiobrightness be below some threshold and that the spectral gradient be negative, should be an effective classifier of frozen soil.

Acknowledgement

This study was supported by NASA Interdisciplinary Research Program Grant NAG5-852.

References

[1] Burke, W.J., T. Schmugge, and J.F. Paris, "Comparison of 2.8- and 21-cm microwave radiometer observations over soils with emission model calculations," J. Geophys. Res., 84, pp.287-294, 1979.

[2] Wang, J.R., T.J. Schmugge, W.I. Gould, W.S. Glazar, and J.E. Fuchs, "A multi-frequency radiometric measurement of soil moisture content over bare and vegetated fields," Geophys. Res. Let., 9, pp. 416-419, 1982.

[3] Schmugge, T.J., "Remote sensing of soil moisture: Recent advances," IEEE Trans. Geosci. Rem. Sensing, GE-24, pp.12-22, 1983.

[4] Camillo, P.J., and T.J. Schmugge, "Correlating rainfall with remotely sensed microwave radiation using physically based models," IEEE Trans. on Geosci. and Rem. Sens., GE-22, pp. 415-423, 1984.

[5] Schmugge, T.J., P.E. O'Neill, and J.R. Wang, "Passive microwave soil moisture research," IEEE Trans. on Geosci. and Rem. Sens., GE-24, pp. 12-22, 1986.

[6] Schmugge, T.J., "Remote sensing applications in hydrology, Rev. Geophys., 25, pp. 148-152, 1987.

[7] Zuerndorfer, B.W., A.W. England, M.C. Dobson, and F.T. Ulaby, "Mapping freeze/thaw boundaries with SMMR data," in press, J. Agricultural and Forest Meteorology, 1989.

[8] Carslaw, H.S., and J.C. Jaeger, Conduction of Heat in Solids, 2nd Ed., Oxford, 1959.

[9] Watson, K., "Geologic application of thermal infrared images," Proc. of IEEE, pp. 128-137, Jan., 1975.

[10] Watson, K., L.C. Rowan, and T.W. Offield, "Application of thermal modeling in the geologic interpretation of IR images," Remote Sensing, K. Watson and R. Regan ed., Geophysics Reprint Series, no. 3, Society of Exploration Geophysicists, 1983.

[11] Kahle, A.B., "A simple thermal model of the Earth's surface for geologic mapping by remote sensing," J. Geophys. Res., 82, pp. 1673-1680, 1977.

[12] Evans, G.W., "A note on the existence of a solution to a problem of Stefan," Quarterly of Applied Mathematics, 9, pp. 185-193, 1951.

[13] Landau, H.G., "Heat conduction in a melting solid," Quarterly of Applied Mathematics, 8, pp. 81-94, 1950.

[14] Douglas, J., and T.M. Gallie, Jr., "On the numerical integration of a parabolic differential equation subject to a moving boundary condition," Duke Mathematical J., 22, pp.557-571, 1955.

[15] Chernous'ko, F.L., "Solution of non-linear heat conduction problems in media with phase changes," International Chemical Engineering J., 10, pp.42-48, 1970.

[16] Hoekstra, P., and A. Delaney, "Dielectric properties of soils at UHF and microwave frequencies," J. Geophys. Res., 79, pp. 1699-1708, 1974.

[17] Hoekstra, P., and W.T. Doyle, "Dielectric relaxation of surface adsorbed water," J. Colloid and Interface Sci., 36, pp. 513-521, 1971.

[18] Hasted, J.B., "Dielectric properties of water and aqueous solutions," Dielectric and Related Molecular Processes, The Chemical Society, London, pp. 121-162, 1972.

[19] Hasted, J.B., Aqueous dielectrics, Chapman and Hall, London, 302p., 1973.

[20] Cole, R.H., and O. Worz, "Dielectric properties of ice," Physics of Ice, N. Riehl, B. Bullemer, and H. Englehardt ed., Plenum, NY, pp. 456-554, 1969.

[21] Camp, P.R., W. Kiszenick, and D. Arnold, "Electrical conduction in ice," Physics of Ice, N. Riehl, B. Bullemer, and H. Englehardt ed., Plenum, NY, pp. 450-470, 1969.

[22] Chandrasekhar, S., Radiative Transfer, Dover, NY, p. 6, 1960.

[23] England, A.W., "Thermal microwave emission from a scattering halfspace," Radio Science, 9, pp. 447-454, 1974.

[24] England, A.W., "Thermal microwave emission from a scattering layer," J. Geophys. Res., 80, pp. 4484-4496, 1975.

[25] Ishimaru, A., Wave Propagation and Scattering in Random Media, I, Academic, NY, p. 11, 1978.

Table 1. Boundary Parameters	
F_{sun}	Solar irradiance = f_1 So (1-A) M(ϕ) cos ϕ
F_{sky}	Sky irradiance = $\sigma T_{sky}^4 + f_2$
F_{wind}	Sensible heat transfer from air to ground $\rho_a c_a C_d$ (W + 2) (T_{air} - T_{ground})
F_{ground}	e σT_g^4
So	Solar Constant = 0.03313 cal/sec^2
A	Albedo
M(ϕ)	Approximate atmospheric transmissivity 1.0 - 0.2 (cos ϕ)$^{-0.5}$ [9][10]
ϕ	Zenith angle
cos ϕ	cos λ cos δ (-cos(2π hour/24)+sin λ sin δ) if > 0, otherwise cos ϕ = 0
λ	local latitude
δ	declination = - 23.433^o cos(2π month/12)
f_1	≈(1-cl) where cl is average cloud cover. Approximation is that some is regained through f_2.
f_2	Irradiance from clouds, approximated as half the average solar irradiance lost in the cloud term, f_1. (cl/2) So (1-A) {$\int$ M(ϕ) cos ϕ dt}/24
σ	Stefan-Boltzmann constant = 1.3533x10^{-12}
T_{air}	Average air temperature To_{air} - T_{del} cos(2π(hour-2)/24) [11]
To_{air}	Monthly average air temperature (e.g., see Fig. 6) T_o - T_1 cos(2π(month-θ_{lag})/12)
T_{del}	Diurnal variation (from meteorological reports)
T_{sky}	T_{air}(0.61 +0.05 w$^{0.5}$)$^{0.25}$ (Brunt's formula, from Kahle [11])
w	Water vapor pressure, mmHg
ρ_a	Air density at surface = 1.25x10^{-3} gm/cm^3
c_a	Specific heat of dry air = .24 cal/gm-K
C_d	Drag coefficient = 0.002+0.006(Z/5000), Z is elevation in meters [11]
W	Wind velocity in m/sec
e	Thermal infrared emissivity
T_g	Soil surface temp from solution to heat flow equation

Table 2. Parameters for Bismarck, ND	
Latitude	47° N
Months	September through December (i.e., 9 - 12)
Soil moisture	10%, 15%, 20% by weight
Cloud cover, cl	20%
Average winds, w	5 m/sec
Albedo	0.2
Thermal IR emissivity, e	0.95
Freeze interval	270-273 K
Dry soil density	1.5 gm/cm^3
Dry soil specific heat	0.2 cal/gm
Dry soil thermal conductivity	0.0005 cal/cm-sec-deg
7% moist soil dielectric constant	3.3
7% moist soil loss tangent	0.23
Average air temperature, T_o	278.3 K (Fig. 6)
Annual air temp variation, T_1	16.9 K deg
Temp phase lag, θ_{lag}	1.12 months
Diurnal temp variation, T_{del}	5 K deg
Water vapor pressure, w	0.76 mmHg

Captions:

Fig. 1. Frequency gradient versus SMMR 37 GHz brightness temperature, Bismarck, North Dakota. Data were collected from 8/1/84 through 12/31/84. Shown with the Bismarck data are clustering decision thresholds for a frozen, mixed, or thawed surface. Based upon ground truth, the solid boxes are frozen, open boxes are thawed, and x's are mixed pixels (personal communication from Zuerndorfer, modified from Zuerndorfer et al. [7]).

Fig. 2. Enthalpy versus Temperature. E(T) and H(T) are approximations to moist soil enthalpy during freezing. H(T) in 2a represents Chernous'ko's, piecewise constant model. The asymmetry of H(T) at each isotherm produces dissimilar heating and cooling performance. H(T) in 2b is the modified model. The symmetry in H(T) at each isotherm produces the necessary similarity for heating and cooling.

Fig. 3. Integration path at constant time. The piecewise constant approximation to H(T) means that the enthalpies, H^- and H^+, are constant between isotherms.

Fig 4. Schematic of emission from a moist soil. Because of the transmissivity of soil, thermal microwave emission originates below its optical surface. If ϕ is the beam angle out of the page, $\phi = \phi' = 0$. $d\omega$ is the solid angle of the beam, $d\omega = d\theta\, d\phi$.

Fig. 5. The complex dielectric constant at 10 GHz as a function of temperature at three water contents for (a) Goodrich clay and (b) Fairbanks silt (from Hoekstra and Delaney [16]).

Fig. 6. Monthly average air temperatures for Bismarck, ND (from National Weather Service data). "Model" refers to the first order Fourier component.

Fig. 7. Temperature versus depth profiles for Bismarck, ND. Curves represent midnight, 6:00 a.m., noon, and 6:00 p.m. for three moisture contents.

Fig. 8. Diurnal soil surface temperatures at Bismarck, ND. Curves represent moisture contents by weight.

Fig. 9. Effective emitting depth versus time of day. Effective emitting depth is equivalent to optical depth in optics, or to 1/2 the skin depth in electromagnetics. Curves represent effective emitting depths for 3 microwave frequencies -- 10.7, 18, and 37 GHz.

Fig. 10. Radiobrightness versus time of day. Curves represent the brightness for 3 moisture contents and at 3 microwave frequencies.

Fig. 11. Radiobrightness spectral gradient versus time of day. Curves represent 3 moisture contents. The gradients are computed as a least squares regression of the radiobrightness at 10.7, 18, and 37 GHz.

Decision Space

1a Bismarck (Day)

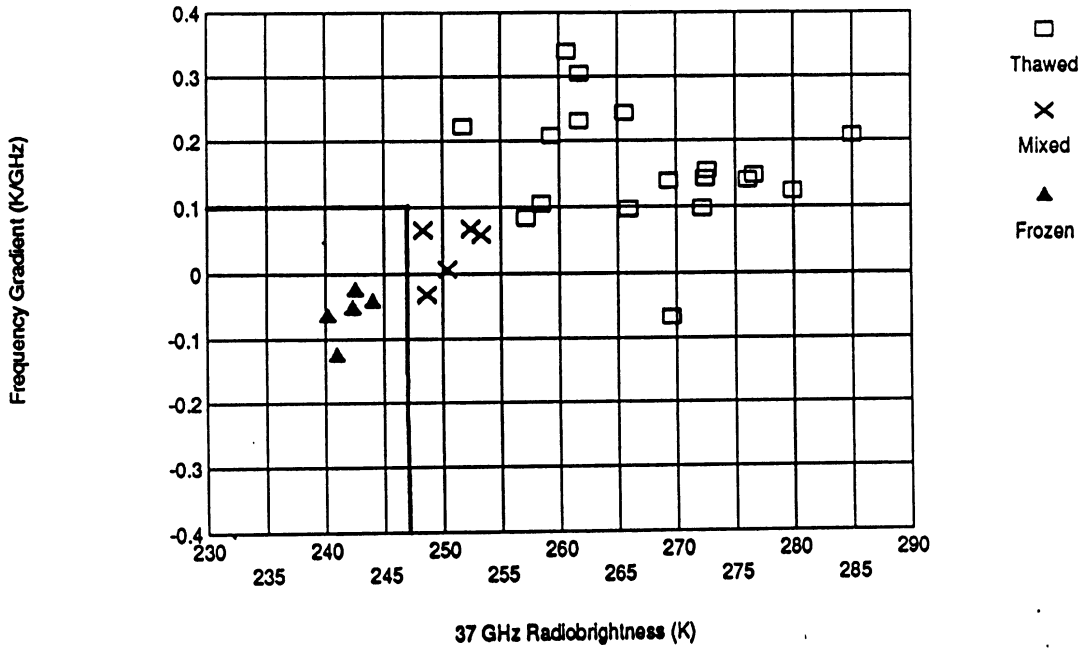

1b Bismarck (Night)

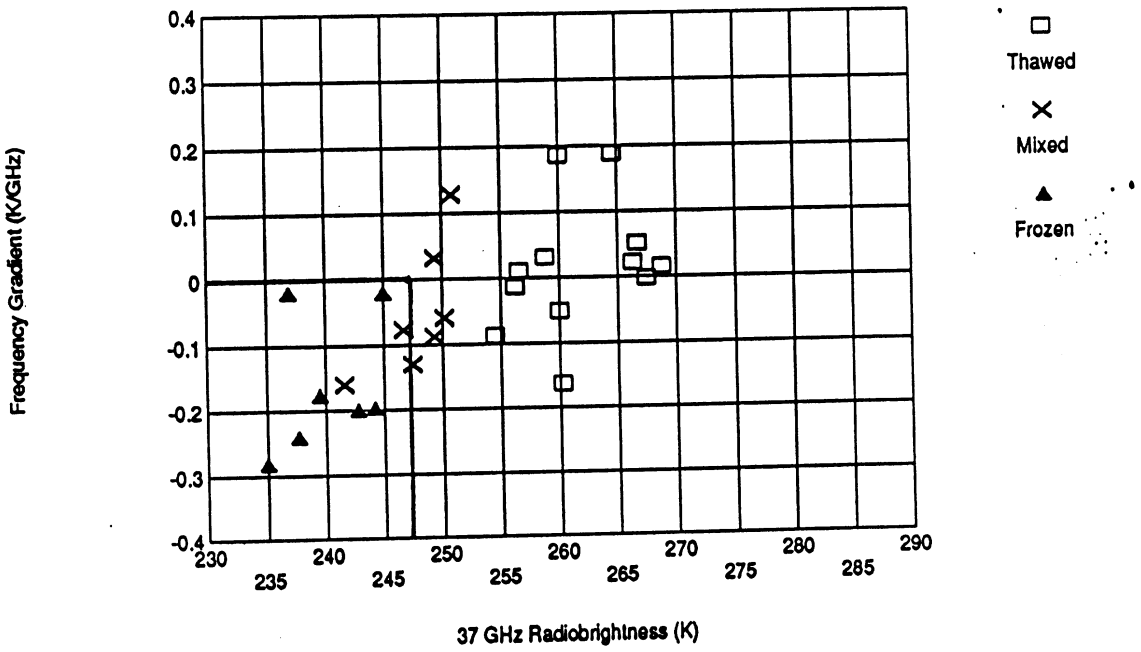

Figure 2a

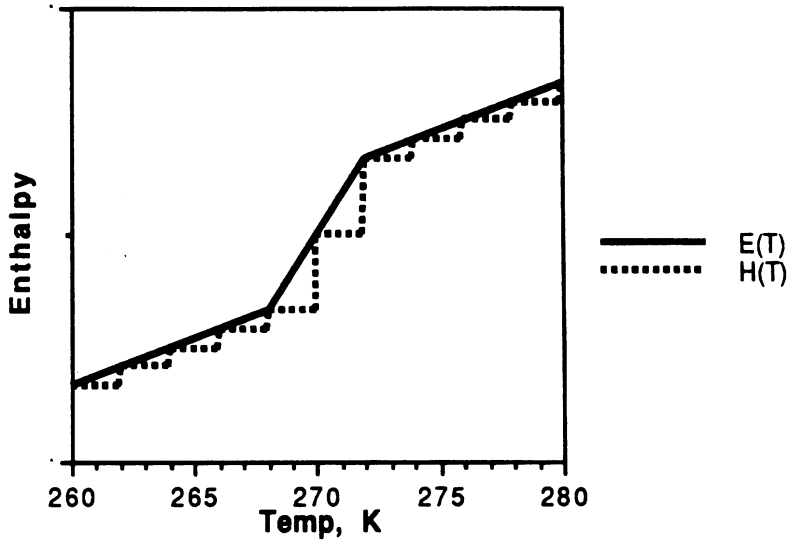

Figure 2b

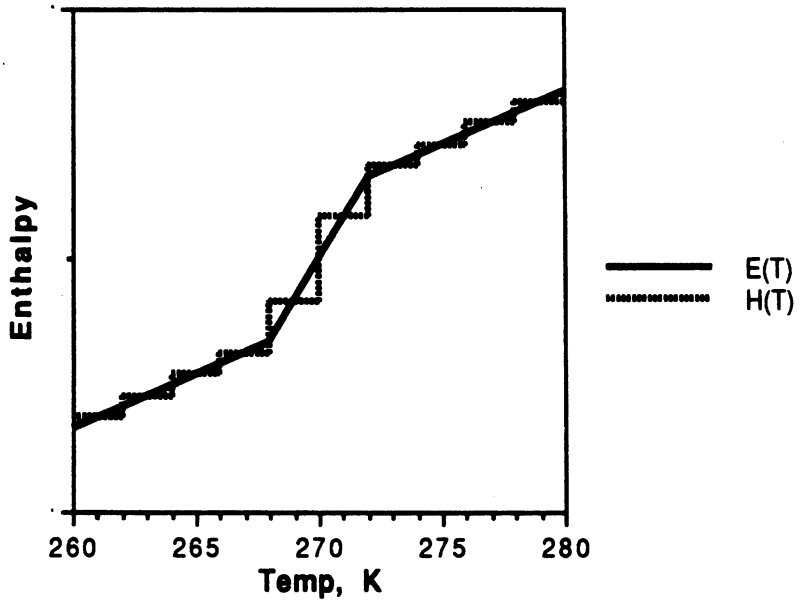

Figure 3

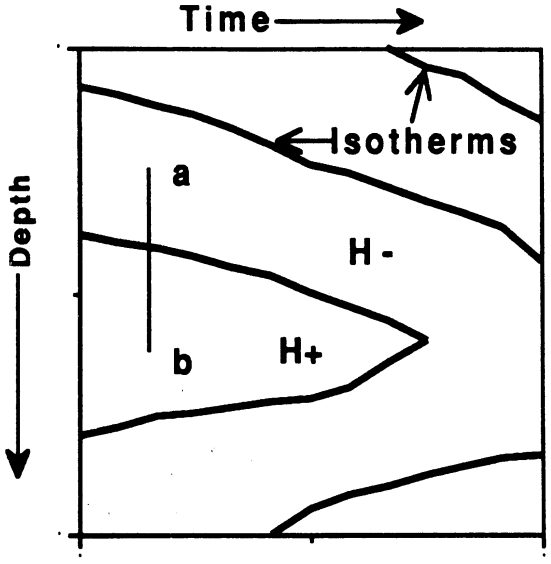

Figure 4

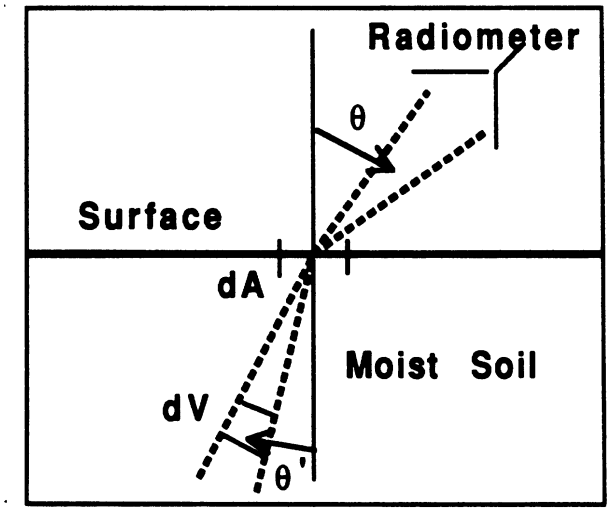

Figure 5a

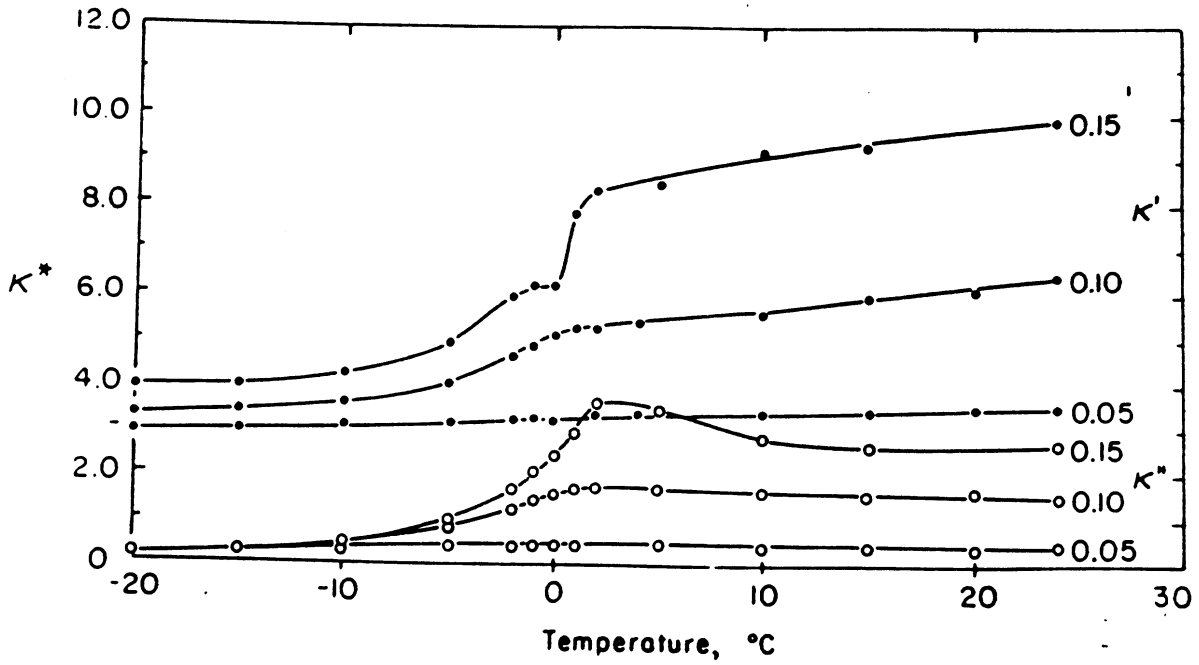

Figure 5b

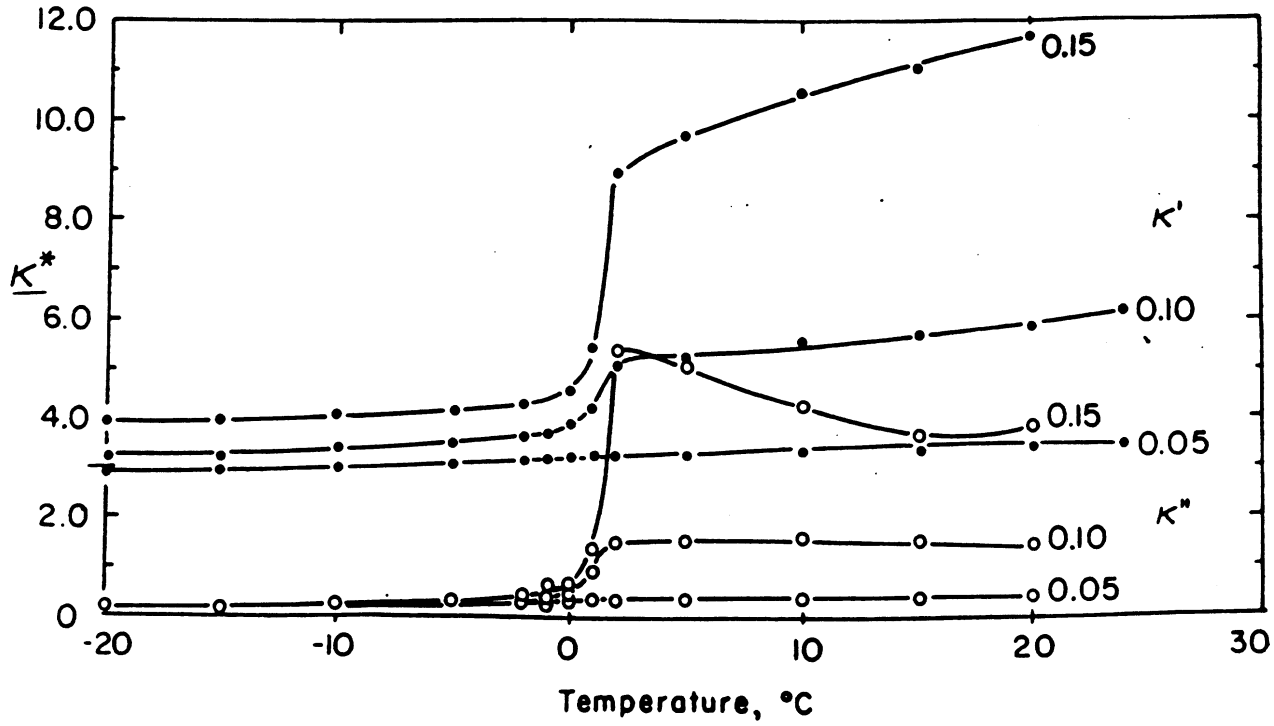

Figure 6

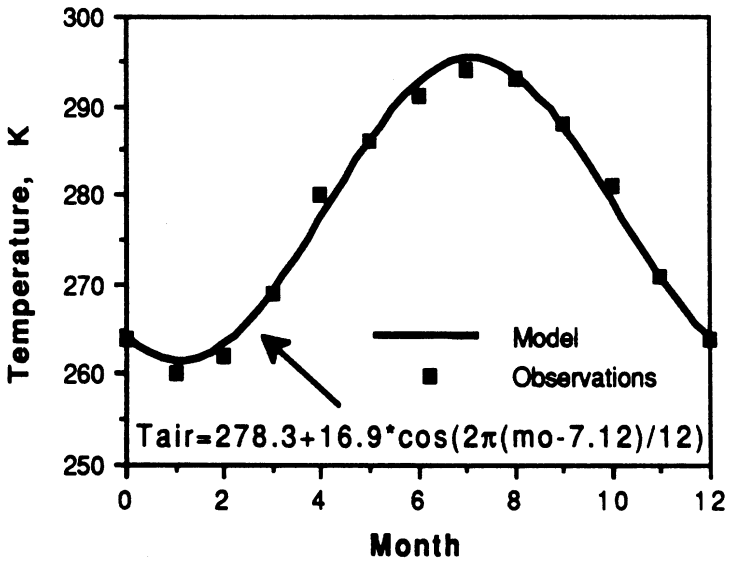
300
290
280
270
260
250
Temperature, K
0
2
4
6
8
10
12
Month
Model
Observations
Tair=278.3+16.9*cos(2π(mo-7.12)/12)

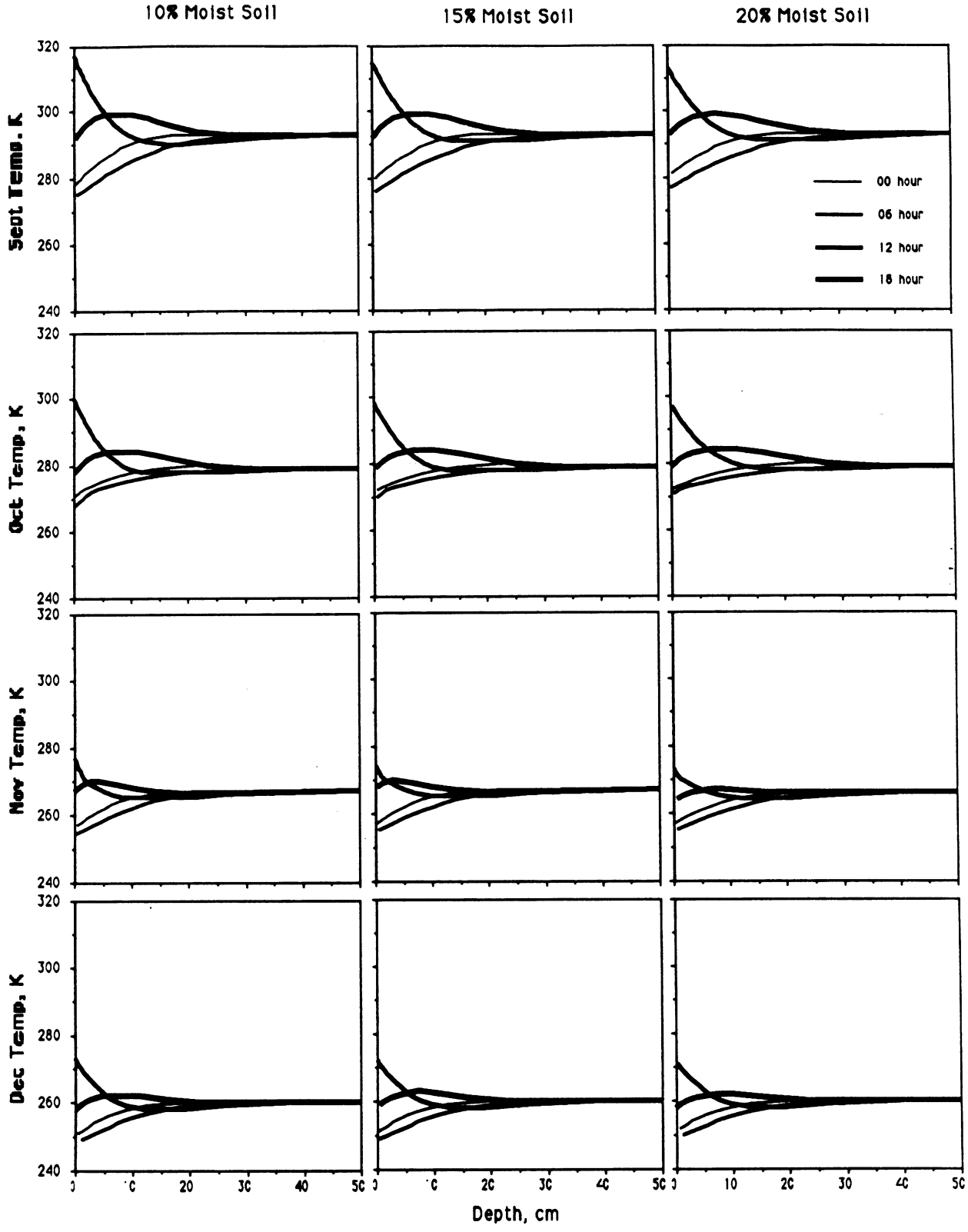
10% Moist Soil
15% Moist Soil
20% Moist Soil
Sept Temp, K
Oct Temp, K
Nov Temp, K
Dec Temp, K
320
300
280
260
240
00 hour
06 hour
12 hour
18 hour
0
10
20
30
40
50
Depth, cm

Fig. 7

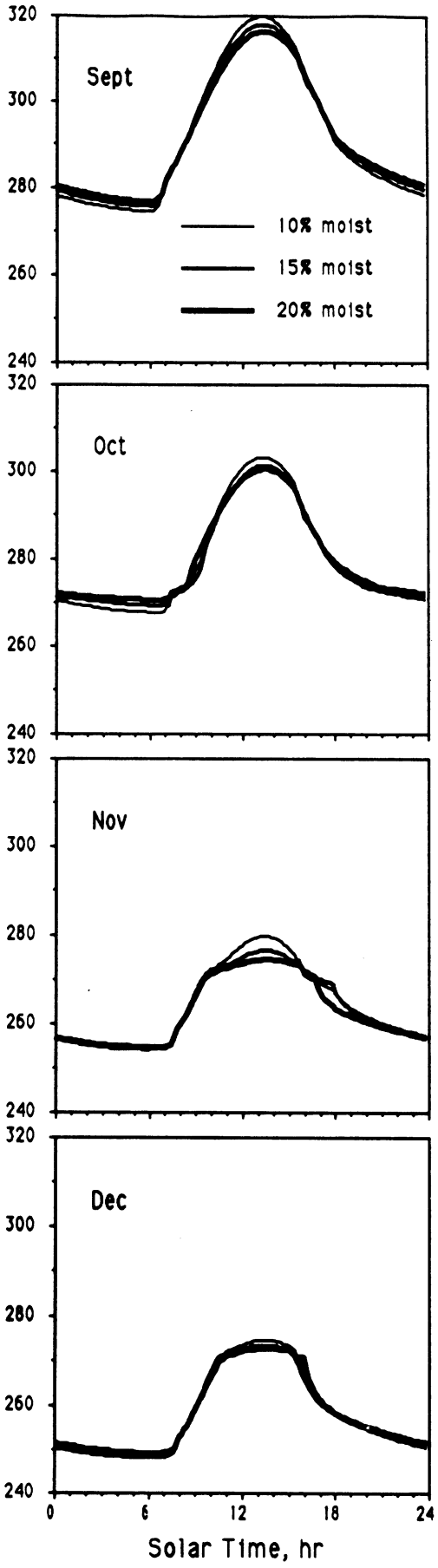
Sept
Oct
Nov
Dec
10% moist
15% moist
20% moist
320
300
280
260
240
0
6
12
18
24
Solar Time, hr

Fig. 8

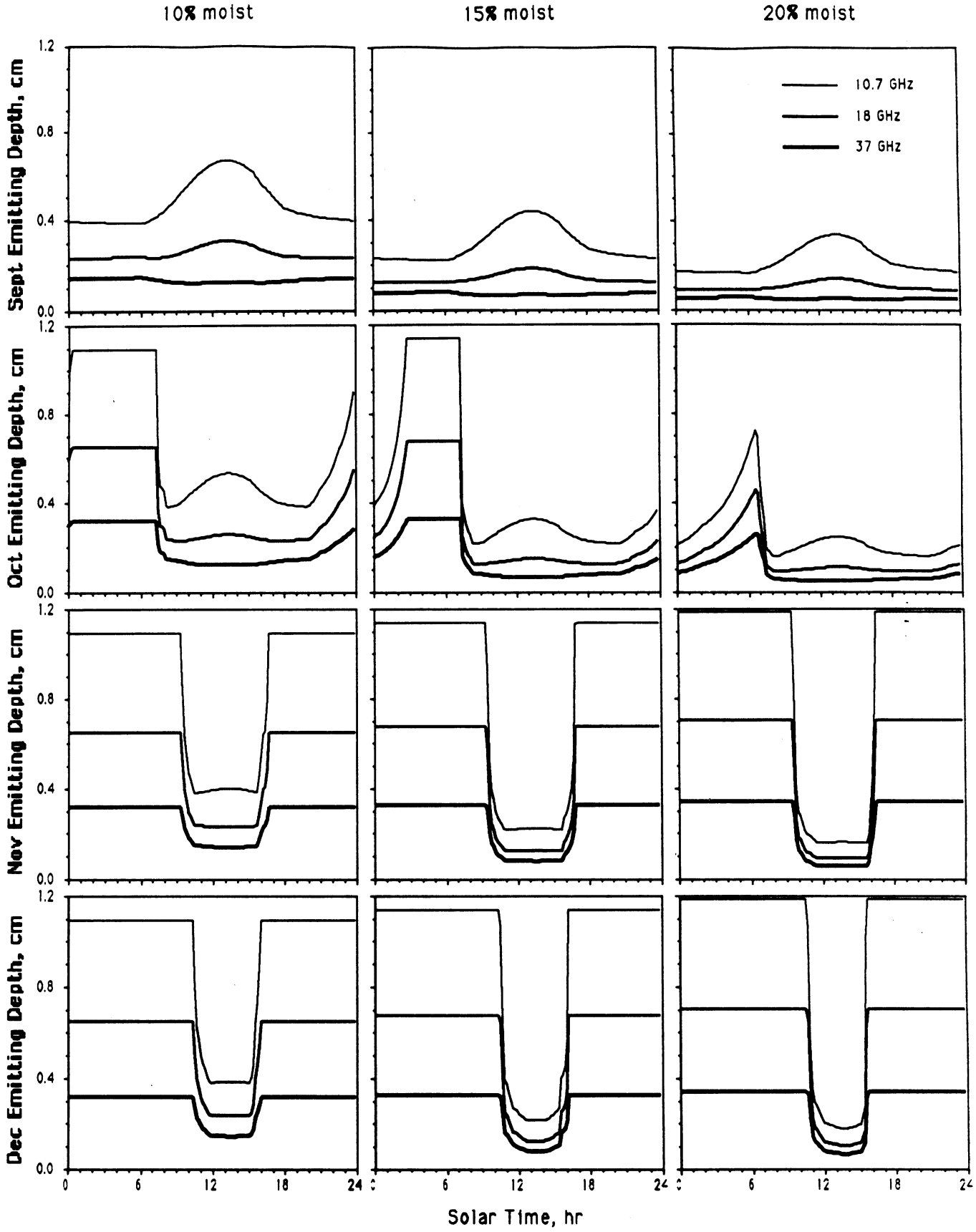
10% moist
15% moist
20% moist
10.7 GHz
18 GHz
37 GHz
Sept Emitting Depth, cm
Oct Emitting Depth, cm
Nov Emitting Depth, cm
Dec Emitting Depth, cm
0.0
0.4
0.8
1.2
0
6
12
18
24
Solar Time, hr

Fig. 9

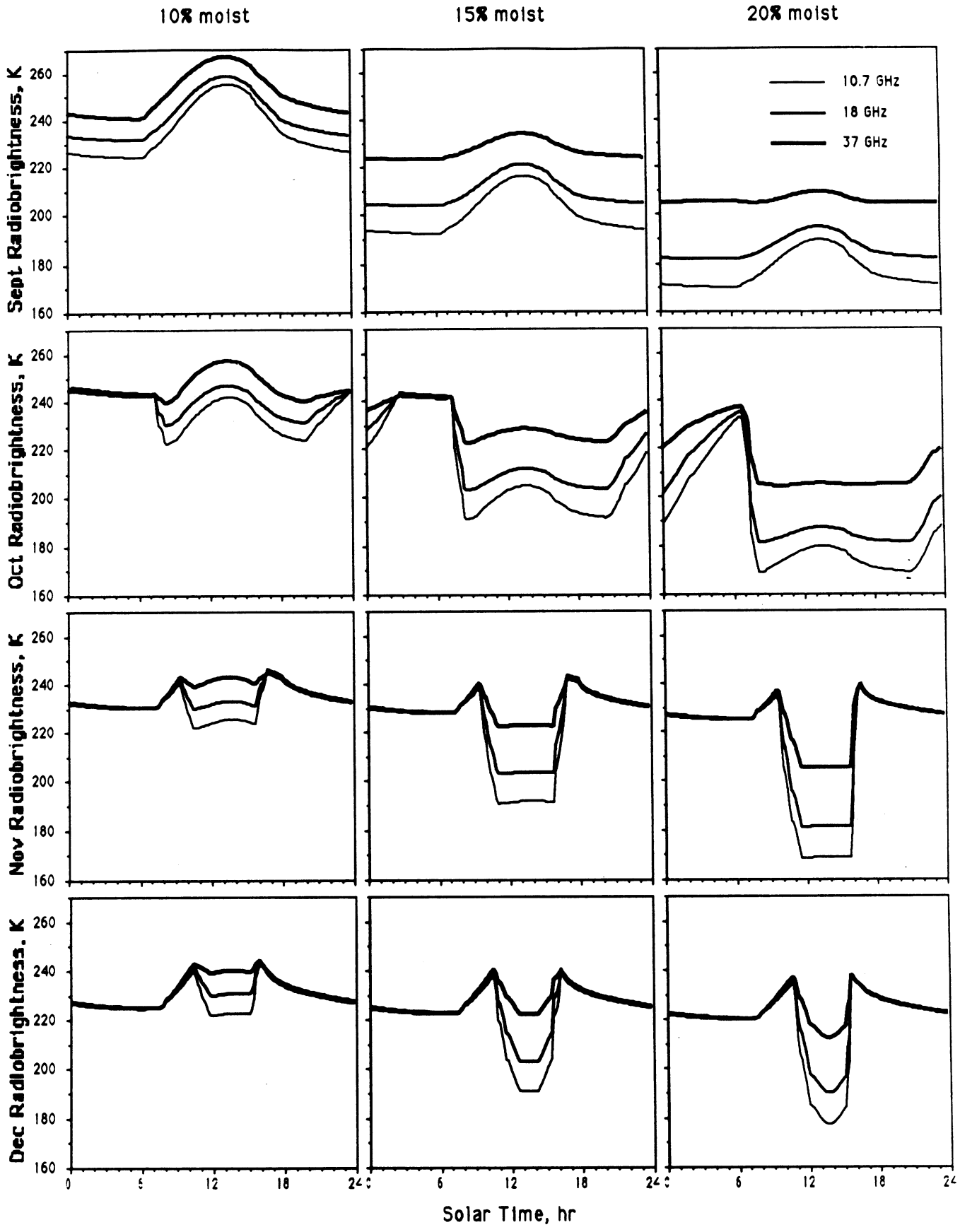
10% moist
15% moist
20% moist
10.7 GHz
18 GHz
37 GHz
Sept Radiobrightness, K
Oct Radiobrightness, K
Nov Radiobrightness, K
Dec Radiobrightness, K
260
240
220
200
180
160
0
6
12
18
24
Solar Time, hr

Fig. 10

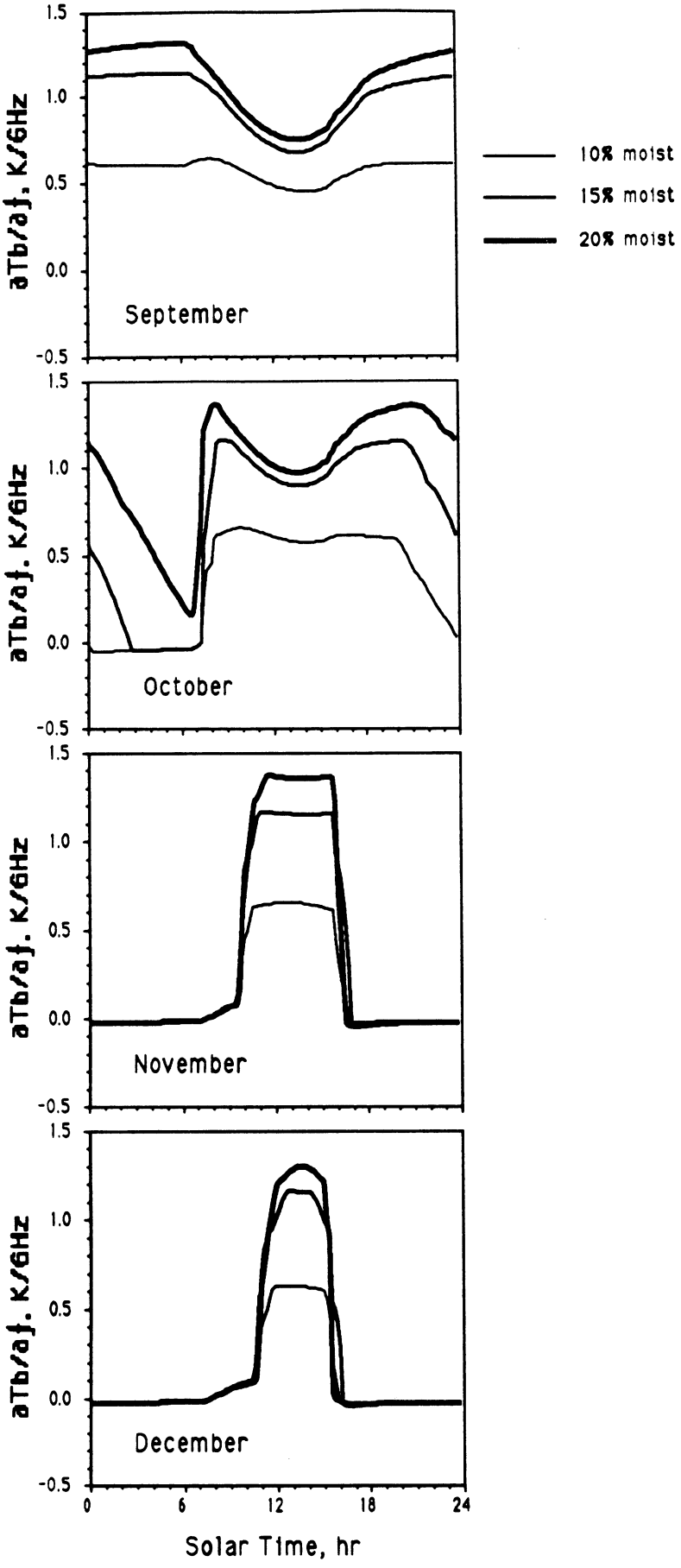
1.5
1.0
0.5
0.0
-0.5
aTb/af, K/6Hz
September
October
November
December
10% moist
15% moist
20% moist
0
6
12
18
24
Solar Time, hr

Fig. 11